

Accepted for the publication in the *Astrophysical Journal*: scheduled for the July-20-2004 issue)

A *Chandra* View of The Morphological And Spectral Evolution of Supernova Remnant 1987A

Sangwook Park

Department of Astronomy and Astrophysics, 525 Davey Lab., Pennsylvania State University, University Park, PA. 16802

park@astro.psu.edu

Svetozar A. Zhekov

Space Research Institute, Moskovska str. 6, Sofia-1000, Bulgaria

David N. Burrows, Gordon P. Garmire

Department of Astronomy and Astrophysics, 525 Davey Lab., Pennsylvania State University, University Park, PA. 16802

and

Richard McCray

JILA, University of Colorado, Box 440, Boulder, CO. 80309

ABSTRACT

We present an update on the results of our monitoring observations of the X-ray remnant of supernova (SN) 1987A with the *Chandra X-Ray Observatory*. As of 2002 December, we have performed a total of seven observations of SN 1987A, which allows us to monitor the details of the earliest stage of the supernova remnant evolution in X-rays. The high angular resolution images from the latest data reveal developments of new X-ray bright spots in the northwestern and the southwestern portions of the remnant as well as changes on the eastern side. The observed soft X-ray flux is increasing more rapidly than ever, and the latest 0.5–2 keV band flux ($f_X \sim 6 \times 10^{-13}$ ergs cm^{-2} s^{-1}) is four times brighter than three years earlier when this monitoring began. The overall X-ray emission is primarily from the blast wave shock with $kT \sim 2.4$ keV. As the blast wave approaches the dense circumstellar material, the contribution from the decelerated slow shock ($kT \sim 0.22$ keV) to the observed X-ray emission is becoming significant. The increase of this slow shock contribution over the last two years is particularly noticeable in the western half of the remnant. These results indicate that the shock front is now

reaching the main body of the inner circumstellar ring and that SN 1987A will be a complete ring with dramatic brightening in coming years. Based on the best-fit two-shock spectral model, we derive approximate densities of the X-ray-emitting regions ($n_e \sim 235 \text{ cm}^{-3}$ for the fast shock and $n_e \sim 7500 \text{ cm}^{-3}$ for the slow shock). There is no direct observational evidence to date for a neutron star associated with supernova remnant 1987A. We obtain an upper limit on the observed X-ray luminosity of any embedded point source ($L_X \leq 1.5 \times 10^{34} \text{ ergs s}^{-1}$) in the 2–10 keV band. The X-ray remnant continues to expand linearly at a rate of 4167 km s^{-1} .

Subject headings: supernovae: general — supernovae: individual (SN 1987A) — supernova remnants — X-rays: general — X-rays: stars

1. INTRODUCTION

Supernova (SN) 1987A, the brightest supernova observed since 1604, occurred in the Milky Way’s satellite galaxy, the Large Magellanic Cloud (LMC). The identification of a blue supergiant (Sanduleak $-69^{\circ}202$, a B3 I star) as the massive progenitor star (Kirshner et al. 1987; Sonneborn et al. 1987) and the detection of the accompanying neutrino burst (Koshiba et al. 1987) indicated that SN 1987A was a Type II core-collapse explosion. A dramatic brightening (up to three orders of magnitude) over the entire electromagnetic spectrum was expected to begin ~ 15 yr after the SN explosion as the shock enters the dense, non-spherically symmetric circumstellar medium (CSM), the so-called “inner ring”, which was produced by the stellar winds from the red supergiant and the blue supergiant phases of the massive progenitor star and then was photoionized by the UV flash from the SN explosion (Burrows et al. 1995; Lundqvist & Fransson 1991; Luo & McCray 1991). At an age of ~ 16 yr (as of 2002 December), optical and X-ray observations clearly show that this event has begun (McCray 2004), signaling the transition of SN 1987A into a supernova remnant (SNR). SN/SNR 1987A is an extremely dynamic object, as the fast blast wave shock ($v \sim 4000 \text{ km s}^{-1}$) begins to heat the inner ring. This remarkable event is the first-ever observation of the “birth” of a supernova remnant.

In the early phases of SNRs, X-ray observations provide effective shock diagnostics such as the electron/ion temperatures, ionization state, electron density, and ISM abundances, as well as useful information on the SN nucleosynthesis. With its unprecedented high angular resolution of $\sim 0''.5$ in X-rays and its moderate spectral resolution (e.g., $E/\Delta E \sim 8$ at $E = 1 \text{ keV}$ for the S3 chip), the Advanced CCD Imaging Spectrometer (ACIS; Garmire et al. 2003) on board the *Chandra X-Ray Observatory* (Weisskopf et al. 1996) is uniquely suited to monitor the rapid morphological and spectral evolution (on the time-scale of months) of the X-ray remnant of SN 1987A.

We have been monitoring SNR 1987A with the *Chandra*/ACIS since 1999 October. As of 2002 December, we have performed a total of seven observations (Table 1). Results from the first six observations have been reported in the literature (Burrows et al. 2000; Park et al. 2002;

Park et al. 2004; Michael et al. 2002). The sub-arcsecond angular resolution of the *Chandra*/ACIS resolved the ring-like X-ray morphology of SNR 1987A, which was interpreted as X-ray emission from the heated ISM between the forward blast wave and the reverse shock (Burrows et al. 2000). The X-ray surface brightness was higher in the eastern side, probably due to an asymmetric SN explosion, although the origin of such an asymmetric explosion is uncertain. We detected X-ray-bright spots in the northeastern and the southeastern portions of the X-ray remnant (Burrows et al. 2000; Park et al. 2002). The locations of these X-ray spots were roughly coincident with the optically-bright spots. The optical bright spots trace where the blast wave shock front cools down and becomes radiative as it encounters dense inward protrusions of the inner ring (Michael et al. 2000). In this model, decelerated, yet non-radiative shocks near the protrusions may also produce soft X-ray emission. The soft X-ray spots positionally coincident with the optical spots were thus consistent with the standard model of the blast wave/inner ring interaction. On the other hand, the fast shock propagating into the tenuous HII region appeared to produce hard X-ray and radio emission with a smoother distribution of surface brightness than those of the soft X-ray and optically bright spots (Park et al. 2002).

The X-ray spectrum was thermal in origin, dominated by line emission from the highly ionized elemental species O, Ne, Mg and Si (Burrows et al. 2000). The X-ray emitting plasma was described with a plane-parallel shock in non-equilibrium ionization (NEI) state with an electron temperature of $kT \sim 3$ keV. A blast wave shock velocity of $v \sim 3500$ km s $^{-1}$ was derived from the Doppler broadening of the detected X-ray line profiles, which indicated an ion temperature of $kT \sim 17$ keV (Michael et al. 2002). This large difference between measured electron and ion temperatures was direct observational evidence for electron-ion non-equilibrium behind the shock in this early phase of the SNR. The observed X-ray flux was increasing non-linearly as the blast wave approached the dense inner ring (Park et al. 2002). The lightcurve was steepening, which indicated the beginning of the predicted dramatic brightening of the SNR (Park et al. 2004). Despite the identification of a core-collapse SN explosion for SN 1987A, no direct evidence for the detection of the associated neutron star has been reported. Only upper limits on the X-ray luminosity for the embedded pointlike source have been estimated (Burrows et al. 2000; Park et al. 2002; Park et al. 2004). We here report on results from the latest *Chandra* observations of SNR 1987A.

2. OBSERVATIONS & DATA REDUCTION

The seven *Chandra* observations of SNR 1987A are presented in Table 1. We first screened all data sets with the flight timeline filter and turned off the pixel randomization for the highest possible angular resolution. We then corrected the spatial and spectral degradation of the ACIS data caused by radiation damage, known as the charge transfer inefficiency (CTI; Townsley et al. 2000), with the methods developed by Townsley et al. (2002a), before further standard data screening by status, grade, and energy selections. The expected effects of the CTI correction include an increase of the number of detected events and improved event energies and energy

resolution (Townsley et al. 2000; Townsley et al. 2002a). “Flaring” pixels were removed and *ASCA* grades (02346) were selected. Photons between 0.3 keV and 8.0 keV were extracted for the data analysis. Lightcurves around the source region were examined for possible contamination from variable background emission and no severe variability was found. The pileup fraction was relatively small (<10%) and thus was ignored in the analysis.

We then applied the “sub-pixel resolution” method (Tsunemi et al. 2001) to improve the angular resolution of the images to better than the CCD pixel size. A typical improvement in the angular resolution by $\sim 10\%$ is expected from this method (Mori et al. 2001). The angular size of SNR 1987A is small (the inner ring is only about $1''.6$ across; e.g., Burrows et al. 1995; Jakobsen et al. 1991), and the ACIS detector pixel size ($0''.492$) is not adequate to fully resolve the remnant. In order to further improve the effective angular resolution of the ACIS images, we deconvolved the images using a maximum likelihood algorithm (Richardson 1972; Lucy 1974) as described in our previous works (Burrows et al. 2000; Park et al. 2002). For the image deconvolution, we used $0''.125$ sky pixels for the data sets with low photon statistics ($\lesssim 1000$ source counts) and $0''.0625$ pixel size for the high statistics data sets ($\gtrsim 1000$ source counts).

3. MORPHOLOGICAL EVOLUTION

In Figure 1, we display the ACIS images of SNR 1987A from the four observations which have the best photon statistics (ObsID 1967, 2831, 2832, and 3829; Table 1). Images from the other three observations with fewer counts have been presented elsewhere (Burrows et al. 2000; Park et al. 2002). These broadband X-ray images clearly exhibit the dynamical nature of this young SNR. The overall surface brightness has doubled over the two-year period (~ 0.09 counts s^{-1} in 2000-12 and ~ 0.19 counts s^{-1} in 2002-12). While the overall flux distribution between the eastern and western sides remains asymmetrical, the latest data reveal the development of new X-ray spots in the northwest and the southwest. New X-ray-bright spots have also developed along the eastern side of the SNR, making the eastern portion of the X-ray ring more smooth than before. The overall X-ray morphology of SNR 1987A thus appears to become a more complete ring during this two year interval. These morphological changes are generally in good agreement with the standard model of the blast wave shock front approaching the dense inner ring (Michael et al. 2000): i.e., the blast wave reached the northeastern side of the inner ring in around 1997 (~ 3700 days after the SN explosion) when the first optical spot emerged (Pun et al. 1997; Garnavich et al. 1997), and it is now reaching the western side of the inner ring. As of 2003 January, the latest optical images taken by the *Hubble Space Telescope (HST)* revealed that optically bright spots have emerged all around the inner ring (McCray 2004). This is a good indication of the blast wave now encountering the inner ring on the western side, a few years after it did on the eastern side. The morphological changes from our *Chandra* data are in good agreement with those in the optical data. We discuss more about this dynamical nature of the blast wave in § 4, based on the spectral analysis results.

Morphological investigations with broad sub-band images have revealed remarkable differences

between the soft and the hard band X-ray emission features (Park et al. 2002). The recent observations with significant photon statistics allow us to repeat this investigation over a larger time base. In Figure 2, we present three sub-band images of SNR 1987A for 2000-12 and 2002-12. Both data contain comparable numbers of photons ($\gtrsim 9000$ counts) so that we can make reliable comparisons on the energy-dependent morphological changes over this two year interval. The sub-bands were chosen primarily to represent the O line features (the 0.3–0.8 keV band, “O-band” hereafter), the Ne line features (the 0.8–1.2 keV band, “Ne-band” hereafter), and the Mg/Si line + any hard-tail emission features (the 1.2–8.0 keV band, “H-band” hereafter). The sub-band boundaries were also chosen to provide comparable photon statistics in each sub-band for reliable comparisons among them. In 2000-12, the O- and Ne-band X-ray emission was bright only in the northeast and the southeast portions of the SNR and these soft X-ray-bright spots were positionally coincident with the optically-bright spots (Figure 2a and Figure 2c). On the other hand, the H-band X-ray emission was nearly anti-correlated with the soft X-ray features and well correlated with the radio bright features (Figure 2e). This remarkable energy-dependent X-ray morphology was interpreted as providing good support for the standard model: i.e., the soft X-ray and optical spots are emission from the slow shock encountering the dense protrusions of the inner ring and the hard X-ray and the radio spots are emission from the fast shock propagating into the low density regions in between the dense protrusions (Park et al. 2002). As of 2002-12, the sub-band X-ray images show more complex features than in 2000-12 (Figure 2), and might not be adequately described by the simple physical interpretation proposed with the 2000-12 data. On the eastern side, the X-ray emission is brighter and now appears to be a continuous arc rather than spatially separated spots in all three sub-bands (Figure 2b, Figure 2d and Figure 2f). On the western side, new soft and hard X-ray spots have emerged, particularly in the northwestern and the southwestern portions of the inner ring. These morphological changes suggest that the blast wave shock front is encountering the main part of the inner ring on the eastern side and that it has begun reaching the dense protrusions on the western side.

The increase in the surface brightness is more outstanding in the Ne- and H-bands compared to the O-band (Figure 2). The count rate ratios between 2002-12 and 2000-12 data, after the quantum efficiency (QE) correction (see § 4), are 1.88 ± 0.05 in the O-band, 2.08 ± 0.04 in the Ne-band, and 2.05 ± 0.05 in the H-band, while the overall 0.3–8.0 keV band count rate ratio is 2.06 ± 0.03 . The count rate increase is more significant in the Ne-band than in the O-band. These differential photon flux increases in the sub-band images suggest spectral changes in the X-ray emitting hot plasma over this two year period.

Considering the rapid propagation of the supernova blast wave, Park et al. (2002) investigated the possibility of detecting radial expansion of the X-ray remnant, and estimated an average angular expansion of $\sim 0.^{\circ}04$ between 1999 October and 2001 April. The measured expansion rate corresponded to a radial velocity of 5200 ± 2100 km s $^{-1}$, with a marginal significance of $\sim 2.5 \sigma$. We now have three more data points for a more reliable estimate of the radial expansion rate of SNR 1987A. We used the same method as described in Park et al. (2002) for this estimate: i.e.,

we constructed radial profiles centered on the mean position of the count distribution (or “center of mass”) with a $0''.05$ annular bin, and then fitted these radial profiles with Gaussians in order to obtain the “peak” radius averaged around the X-ray ring. The best-fit Gaussian peak radii versus time are displayed in Figure 3. The peak radius increases by $\sim 0''.06$ from 1999 October to 2002 December. The best-fit expansion rate of SNR 1987A, indicated by the solid line in Figure 3, is $4167 \pm 773 \text{ km s}^{-1}$, which confirms the previous estimate (Park et al. 2002) with higher significance ($\sim 5.4 \sigma$). We note that the X-ray emission is most likely generated between the forward and the reverse shock, but the bright X-ray features appear to be dominated by emission from the forward shock approaching the dense inner ring. The estimated radii, whose measurements are significantly affected by the positions of the bright X-ray-emitting features, therefore presumably trace the high emissivity region as the blast wave progresses into the dense CSM, rather than measuring the actual movement of the X-ray-emitting material. The blast wave shock front is likely slowing down as it sweeps through the dense CSM, at least along the inner ring. Upcoming *Chandra* observations will be monitored for deviation from linear expansion, which would provide direct evidence for deceleration of the shock front.

4. SPECTRAL EVOLUTION

The four *Chandra*/ACIS observations with good statistics (ObsID 1967, 2831, 2832, and 3829; Table 1) (~ 6000 – 9000 counts) allow us to investigate spectral changes of the SNR over a period of 24 months. We extracted the source spectrum of SNR 1987A from a circular region with a $2''$ – $3''$ radius for each of the four observations. The background was estimated from a surrounding annulus with an inner radius of $3''.5$ – $4''$ and an outer radius of $7''.5$ – $10''$. Each spectrum has been binned to contain a minimum of 50 counts per channel. For the spectral analysis of our CTI-corrected data, we have utilized the response matrices appropriate for the spectral redistribution of the CCD, as generated by Townsley et al. (2002b). The low energy ($E \lesssim 1 \text{ keV}$) QE of the ACIS has degraded because of molecular contamination on the optical blocking filter. We corrected this time-dependent QE degradation by modifying the ancillary response function for each extracted spectrum, utilizing the IDL ACISABS software¹.

We fitted individual X-ray spectra of SNR 1987A with an NEI plane-parallel shock model (Borkowski et al. 2001), and found that fitted parameters were similar among all four spectra. We can therefore obtain the best limits on the parameters by performing a combined fit to the four spectra, making the assumption that both N_H and the elemental abundances are constant during this time interval (the statistics are not good enough to detect abundance variations). The spectral contributions from the elements He, C, Ca, Ar, and Ni are insignificant in the fitted energy range (0.4–5.0 keV), so we fixed the abundances of these elements at plausible values. He and C were

¹For a discussion of this instrumental issue, see http://cxc.harvard.edu/cal/Acis/Cal_prods/qeDeg/index.html. The software was developed by George Chartas and is available at <http://www.astro.psu.edu/users/chartas/xcontdir/xcont.html>.

set to the abundances appropriate for the inner circumstellar ring (Lundqvist & Fransson 1996): He = 2.57 and C = 0.09, relative to solar abundances (Anders & Grevesse 1989). We fixed the Ca (= 0.34), Ar (= 0.54) and Ni (= 0.62) abundances to values appropriate for the LMC ISM (Russell & Dopita 1992) because the ring abundances were unavailable for these elemental species in Lundqvist & Fransson (1996). The elements N, O, Ne, Mg, Si, S, and Fe typically have significant effects on the X-ray spectral shape in the fitted energy band, and we therefore use the X-ray observations to measure these abundances directly in SNRs. In fact, X-ray line emission from the most of these species was detected from the dispersed spectrum (Michael et al. 2002), although the poor photon statistics did not allow firm measurements of these elemental abundances. Nonetheless, earlier ACIS data indicated that fixing these elemental abundances at the ring or LMC values could not adequately describe the observed X-ray spectrum of SNR 1987A (Michael et al. 2002). We allowed the abundances of these elements to vary freely, but constrained them to be the same for all four spectra. The temperature and emission measure, on the other hand, were allowed to vary freely between the four spectra. The best-fit column density is $N_H = 1.7_{-0.3}^{+0.2} \times 10^{21} \text{ cm}^{-2}$ (2σ uncertainties are quoted throughout this paper). The results of this spectral fitting are summarized in Table 2 and Table 3. In Figure 4, we present the X-ray spectra of SNR 1987A from data taken on 2000-12 and 2002-12. The best-fit NEI shock model is overlaid onto each spectrum. Figure 4 shows that the overall spectral shape has not changed significantly as the X-ray flux increased over the past two years. While the temporal variation of the ionization timescale is uncertain with the current data, the increase in the emission measure is substantial (Table 3). There also appears to be a monotonic decrease in the electron temperature for the last two years (Table 3). Figure 5 displays these temporal variations of the electron temperature and the volume emission measure. These overall variations of the electron temperature and the emission measure are typical signatures of a shock slowing down by encountering dense material, which is in good agreement with the standard model of the blast wave-inner ring interaction for SNR 1987A.

As the blast wave begins to interact with the dense inner ring, the X-ray spectrum is expected to show evidence for increasing contributions from slow shocks ($v \sim 500 \text{ km s}^{-1}$) (Michael et al. 2002). In fact, our spectral analysis with a single temperature model suggested a decrease of the best-fit electron temperature over the past two years. We thus examined the slow shock contribution by fitting the latest spectrum (2002-12) with a two-temperature model. We forced elemental abundances and the foreground column to be the same for both the soft and hard components, while allowing the electron temperature, ionization timescale, and emission measure to vary separately for each component. The fitted abundances are generally consistent with those obtained above. We found that the soft component indicated a highly advanced ionization state ($n_{et} \sim 10^{13} \text{ cm}^{-3} \text{ s}$), and can be described by a thermal plasma in collisional ionization equilibrium (CIE). We thus repeated the spectral fitting with a CIE soft component + an NEI hard component by fixing elemental abundances at the best-fit values as presented in Table 2 (Figure 6). The best-fit parameters from this two-component model fit for the 2002-12 data are presented in Table 4. While the implementation of this two-temperature model was physically motivated by considering the shock-CSM interaction, the presence of the additional soft component appears to be supported by the statistics as well: i.e.,

we separately fitted the 2002-12 data with a single temperature NEI model ($\chi^2/\nu = 115.84/101$), and an F-test suggested that the statistical improvement in the fit with the two-temperature model is significant (F-probability is $\sim 4 \times 10^{-5}$). The best-fit foreground absorption ($N_H \sim 2.3 \times 10^{21} \text{ cm}^{-2}$) is some $\sim 30\%$ higher than that from the single-temperature model fit ($N_H \sim 1.7 \times 10^{21} \text{ cm}^{-2}$), which is perhaps expected with the addition of the soft component. The higher absorption is in better agreement with that measured by UV spectroscopy ($N_H \sim 3 \times 10^{21} \text{ cm}^{-2}$; e.g., Fitzpatrick & Walborn 1990), and is presumably more realistic. The low electron temperature ($kT = 0.22 \text{ keV}$) for the soft component implies a significantly decelerated shock velocity of $v \sim 400 \text{ km s}^{-1}$ (assuming an electron-ion equilibrium for this component, as supported by its CIE state). The X-ray flux from the slow shock provides $\sim 18\%$ of the total flux in the 0.5–10 keV band.

Based on the measured *EMs* (Table 4), it is evident that the electron density for the soft component is higher than that for the hard component, even assuming the “same” X-ray-emitting volume for each component. We can estimate the densities for the X-ray-emitting regions by considering reasonable geometries for the emission volumes. For the fast shock component ($kT = 2.44 \text{ keV}$), we assume a simple geometry of a spherical shell with an inner radius of $0''.6$ (i.e., $\sim 4.5 \times 10^{17} \text{ cm}$ at the LMC distance of 50 kpc) where the blast wave began to enter the HII region at an age of ~ 1200 days (Manchester et al. 2002). Assuming the blast wave has been propagating at a constant velocity of $\sim 3000 \text{ km s}^{-1}$ (Manchester et al. 2002) since then, the outer radius is $0''.76$ or $\sim 5.7 \times 10^{17} \text{ cm}$ as of 2002-12 (5791 days). We also assume $n_e \approx 1.5 n_H$ for the ring abundances (e.g., Masai & Nomoto 1994). An electron density of $n_e \sim 235 \text{ cm}^{-3}$ is then derived from the best-fit emission measure of the hard component (Table 4). The density of the dense CSM that slows down the blast wave to produce the bulk of the soft X-ray emission is more difficult to estimate because this dense region, containing the inward protrusions, is not resolved and thus the geometry of the X-ray-emitting volume is uncertain. Since the optical spots are now present all around the inner ring and the soft X-ray emission appears to be more continuous along the X-ray ring than ever, we make a simple assumption of a shell-like soft X-ray-emitting region. This soft X-ray emission is most likely from along the inner ring, whose thickness is $\sim 0''.088$ ($\sim 0.02 \text{ pc}$ at the distance of 50 kpc; Jakobsen et al. 1991). Considering this ring-like geometry, we may thus use a cylindrical shell with the ring thickness for the soft component instead of a spherical shell. We assumed a fast shock velocity of 3000 km s^{-1} between days 1200 and 3700, when the shock began interacting with the CSM and slowed down to 400 km s^{-1} . With these assumptions, the inner radius of the cylindrical shell is $\sim 5.0 \times 10^{17} \text{ cm}$ and its outer radius is $\sim 5.1 \times 10^{17} \text{ cm}$. The estimated average thickness of the dense CSM ($\sim 10^{16} \text{ cm}$) is consistent with the “characteristic dimension” of optical spot 1 (Michael et al. 2000). With this geometry for the X-ray-emitting region, the best-fit volume emission measure for the soft component (Table 4) implies an electron density of $n_e \sim 7500 \text{ cm}^{-3}$. Previous estimates of the densities for the HII region and the inner ring are on the order of $\sim 10^2 \text{ cm}^{-3}$ and $\sim 10^4 \text{ cm}^{-3}$, respectively (Chevalier & Dwarkadas 1995; Borkowski et al. 1997; Lundqvist & Fransson 1996). Considering the systematic uncertainties in the adopted geometries and the fact that the blast wave might not have encountered the densest portion of the inner ring yet, the derived densities are in good

agreement with the previous results.

The latest X-ray images reveal the development of new X-ray spots on the western side of the SNR, which suggests that the blast wave is approaching the inner ring in the west as well as in the east (§ 3). In order to quantitatively investigate this hypothesis, we performed two-component model fitting for the eastern and western halves of the SNR, and compared the results between 2000-12 and 2002-12. Because of the small angular size and the apparent asymmetric flux distribution of the SNR, defining the “eastern” and the “western” halves is dependent on how we determine the center of the SNR (e.g., the “center of mass” of the intensity distribution vs. the geometrical center; Michael et al. 2002). Our purpose in performing this spectral analysis by halves is to compare the flux variations between 2000-12 and 2002-12, presumably caused by the emergence of the new X-ray spots in the western side. For this purpose, we chose centers close to the positions of the faintest X-ray flux near the geometrical center of the remnant based on the broadband images. The eastern and western halves of the SNR, determined by these “centers”, are intended to effectively separate the bright X-ray spots in the northeastern and northwestern sides of the X-ray ring. The best-fit spectral parameters for the two halves are generally consistent with those from the entire remnant, although less constrained due to the reduced photon statistics. The X-ray flux variations between the eastern and western sides of SNR 1987A for the last two years are presented in Table 5. We found that the 0.5–10 keV band X-ray flux from the slow shock (the soft spectral component) has marginally increased by $\sim 35\%$ in the eastern half between 2000 and 2002. By contrast, the X-ray flux from the slow shock in the western half has significantly increased by a factor of more than 5 for the same time period. For comparison, the observed X-ray flux originating from the fast shock (the hard spectral component) has only increased by a factor of ~ 2 in both the eastern and the western halves. These differential flux changes between the eastern and the western sides of the SNR indicate that the blast wave has reached the dense inner ring and is slowing down in the western side of the SNR some ~ 5 years after it did in the eastern side when the first optical spot emerged.

5. X-ray Lightcurve

A non-linear increase of the X-ray flux from SNR 1987A over the last decade has been reported (Park et al. 2002; Park et al. 2004). We present the latest X-ray lightcurve of SNR 1987A by combining the *ROSAT* and *Chandra* data (Table 6; Figure 7). The *ROSAT* data were obtained from Hasinger, Aschenbach, & Trümper (1996). The first four *Chandra* fluxes have been updated by correcting the QE for contamination, which had not been characterized at the time of Park et al. (2002). The QE correction resulted in some $\sim 6\%–20\%$ increase in the estimated X-ray fluxes for those four *Chandra* observations (Park et al. 2004). With the earlier observations, only single-temperature models were feasible because of the poor photon statistics. For consistency, we present the soft X-ray fluxes estimated from the single-temperature NEI model for all seven *Chandra* observations in Table 6 and Figure 7. As of 2002-12, the 0.5–2 keV band X-ray flux from

SNR 1987A is $f_X \sim 5.95 \times 10^{-13}$ ergs cm $^{-2}$ s $^{-1}$, which is nearly four times brighter than 1999-10 when we began this monitoring observations with *Chandra*.

The X-ray flux increase rate has apparently been steepening, and cannot be fitted with simple linear or quadratic functions. We thus attempted more complex non-linear models to fit the lightcurve. Here we present a simple model of a blast wave propagating into an exponentially increasing density distribution. The X-ray flux can be expressed as $f_X \propto n_e^2 V T^{-0.6}$ for $0.01 \text{ keV} < kT < 3.4 \text{ keV}$, where V is the X-ray emission volume (e.g., McKee & Cowie 1977). We assumed $V \propto R^3$ (where R is the radial distance from the center of the SNR) and a constant T . We note that the electron temperature appears to be decreasing during this period (§ 4), but this decrease is small and we assume a constant temperature for the purpose of this simple fit. (The measured temperature change between 2000-12 and 2002-12 would imply only $\sim 10\%$ change in the X-ray flux estimate.) The blast wave propagates through a low-density HII region before encountering the high-density inner ring; thus we expect an intermediate density region at the transition between the HII region and the inner ring. We assumed an exponential density distribution along the radius of the SNR in this transition region. The X-ray flux is then

$$f_X \propto R^3 (n_0 + n_r e^{-\frac{R_r - R}{D}})^2, \quad (1)$$

where n_0 is the electron density in the HII region, R_r is the radius of the inner ring, n_r is the electron density of the inner ring at $R = R_r$, and D is a characteristic *scale height* of the exponential density distribution. Now, we define R_0 as the radius at which the blast wave started to interact with the HII region, t as the time since the SN explosion, v as the shock velocity, and t_0 as t at $R = R_0$. We can then rewrite equation (1) as

$$f_X = f_0 [1 + \beta(\tau - 1)]^3 [1 + q e^{-\frac{\alpha-1-\beta(\tau-1)}{s}}]^2, \quad (2)$$

where f_0 is the X-ray flux at $t = t_0$, $\tau \equiv \frac{t}{t_0}$, q is the density ratio between the inner ring and the HII region $\frac{n_r}{n_0}$, $s \equiv \frac{D}{R_0}$ is a modified characteristic scale, α is the radius ratio of $\frac{R_r}{R_0}$, and $\beta \equiv \frac{v t_0}{R_0}$. Based on the radio data (Manchester et al. 2002), we chose $R_0 = 0''.6$, $v = 3000 \text{ km s}^{-1}$, and $t_0 = 1200$ days since the SN explosion. We adopted $R_r = 0''.83$ from the optical data (e.g., Jakobsen et al. 1991). We can therefore fit the X-ray lightcurve in terms of f_0 , q , and s . The best-fit parameters are $f_0 = (8.0 \pm 2.0) \times 10^{-15}$ ergs cm $^{-2}$ s $^{-1}$, $\frac{n_r}{n_0} = 17.6 \pm 1.9$, and $D = 0''.057 \pm 0''.003$ with $\chi^2/\nu = 7.4/11$. This best-fit model is displayed as a dashed-curve in Figure 7. The fitted f_0 is in good agreement with the *ROSAT* data. The best-fit density ratio is considerably lower than the estimates from the modeling of previous observations in other wavelengths (typically $\frac{n_r}{n_0} \sim 100$; e.g., Chevalier & Dwarkadas 1995; Borkowski, Blondin, & McCray 1997; Lundqvist & Franssen 1996). While it is possible that this is due to the simplicity of our model, we note that this density ratio is also consistent with that derived from our spectral analysis (§ 4) within a factor of ~ 2 .

The data points used in our fit are *incomplete*: i.e., the blast wave shock front has not yet swept through the densest portions of the ring, hence our X-ray lightcurve has not yet peaked. We thus expect even steeper flux increases with upcoming data.

6. Neutron Star

The identification of SN 1987A as a core-collapse SN explosion, as evidenced by the massive, blue supergiant progenitor star and by the detection of the neutrino burst coincident with the SN explosion, predicts the existence of a compact remnant, most likely a neutron star, at the center of the SNR. However, we have not detected X-ray emission from the embedded central point source. This non-detection of the central point source is not surprising because the stellar debris from the SN explosion is expected to remain opaque in the radio through X-ray wavelengths for decades after the SN event (Fransson & Chevalier 1987). We have estimated upper limits for the X-ray emission from the embedded point source by simulating a point source at the center of the observed X-ray images of SNR 1987A using the Monte Carlo technique described previously (Burrows et al. 2000; Park et al. 2002). We obtain a 90% confidence upper limit for the unabsorbed X-ray luminosity, $L_X = 1.5 \times 10^{34}$ ergs s $^{-1}$, in the 2–10 keV band for any embedded central point source, somewhat lower than previous limits.

7. Summary & Future

As of 2002 December, we have performed a total of seven observations of SNR 1987A with the *Chandra*/ACIS. With superb angular resolution and moderate spectral resolution, the *Chandra*/ACIS data have provided a unique opportunity to monitor the morphological and spectral evolution of the X-ray remnant of SN 1987A. The X-ray remnant is ring-like with an asymmetric flux distribution between the eastern and western sides. The overall broadband surface brightness has doubled between 2000 December and 2002 December. We detected the development of new X-ray-bright spots in the western side of the remnant in addition to the previously-known features in the eastern side. The X-ray emission features in the eastern side are now more continuous than before, while new X-ray spots are emerging in the western side. These morphological changes appear to indicate that the blast wave is approaching closer to the main portion of the dense inner ring. We detect an average angular expansion of $\sim 0''.06$ between 1999 October and 2002 December, which corresponds to an average radial velocity of $v \sim 4167$ km s $^{-1}$ for the last four years.

Our spectral analysis suggests that the average electron temperature of the shock has been decreasing, whereas the observed flux significantly increased. The best-fit elemental abundances are generally consistent with those of the LMC ISM, and thus the X-ray emission in SNR 1987A appears to be dominated by that from the shocked ISM rather than shocked metal-rich ejecta. A two-temperature shock model indicates that the contribution from the decelerated (by the dense CSM) slow shock ($v \sim 400$ km s $^{-1}$) to the observed X-ray flux is $\sim 18\%$ of the total flux as of 2002 December. It is notable that the slow shock contribution has increased more significantly in the western side than in the eastern side since 2000 December. This spectral evolution is consistent with the morphological evolution. Both imply that the blast wave is now encountering the dense circumstellar material in the western side in addition to the eastern side. Based on the two-

temperature model, we derive electron densities $n_e \sim 235 \text{ cm}^{-3}$ for the hard X-ray emission ($kT = 2.44 \text{ keV}$) from the fast shock and $n_e \sim 7500 \text{ cm}^{-3}$ for the soft component ($kT = 0.22 \text{ keV}$) from the slow shock decelerated by the dense inner ring.

The X-ray lightcurve has been steepening rapidly since 2000. As of 2002 December, the 0.5–2 keV band X-ray flux ($f_X \sim 6 \times 10^{-13} \text{ ergs cm}^{-2} \text{ s}^{-1}$) is nearly four times brighter than in 1999 October when this monitoring program began. We fit the X-ray lightcurve with a non-linear model by assuming an exponential density distribution in the transition regions between the HII region and the inner ring. The best-fit model implies a density contrast of ~ 17 between these two regions, which is consistent with the density estimates from the spectral fitting. This result is also in plausible agreement with the previous density estimates.

Our results clearly demonstrate the extremely dynamic nature of SNR 1987A. The morphological and spectral characteristics are rapidly changing on a time scale of months. Moreover, the latest information obtained by our *Chandra* data strongly indicates that the predicted dramatic brightening (up to nearly three orders of magnitude), as the blast wave sweeps through the dense CSM, might be underway. This remarkable event represents the first-ever observation of the *birth of a supernova remnant*. This monitoring program of SNR 1987A should thus continue in coming years. In addition to the imaging observations, high spectral resolution grating observations with *Chandra* and *XMM-Newton* should be performed in order to determine the details of the shock parameters such as the electron/ion temperatures, ionization states, the elemental abundances, and the 3-dimensional structure of the blast wave shock and the ejecta material.

Although the creation of a compact remnant, probably a neutron star, is expected from the identified core-collapse explosion for SN 1987A, we have yet to detect direct observational evidence for a central pointlike source. This non-detection of a point source appears to be caused by the cold, dense stellar debris around the center of the SNR, which will most likely remain optically thick in the X-ray band for more than a decade. We obtain an upper limit on the observed 2–10 keV X-ray luminosity from any embedded central point source of $L_X \sim 1.5 \times 10^{34} \text{ ergs s}^{-1}$.

The authors thank P. Challis and the Supernova INTensive Study (SINS) collaboration for providing their *HST* images. We also thank D. Manchester and B. Gaensler for providing the radio images taken with *ATCA*. This work was supported in part by NASA under contract NAG8-01128 and by SAO under grant GO1-2064b and GO2-3098a.

REFERENCES

Anders, E. & Grevesse, N. 1989, *Geochim. Cosmochim. Acta*, 53, 197
Borkowski, K. J., Blondin, J. M., & McCray, R. 1997, *ApJ*, 476, L31
Borkowski, K. J., Leyerly, W. J., & Reynolds, S. P. 2001, *ApJ*, 548, 820

Burrows, C. J., Krist, J., Hester, J., Sahai, R., Trauger, J. T., Stapelfeldt, K. R., Gallagher III, J. S., Ballester, G. E., Casertano, S., Clarke, J. T., Crisp, D., Evans, R. W., Griffiths, R. E., Hoessel, J. G., Holtzman, J. A., Mould, J. R., Scowen, P. A., Watson, A. M., & Westphal, J. A. 1995, *ApJ*, 452, 680

Burrows, D. N., Michael, E., Hwang, U., McCray, R., Chevalier, R. A., Petre, R., Garmire, G. P., Holt, S. S., & Nousek, J. A. 2000, *ApJ*, 543, L149

Chevalier, R. A. & Dwarkadas, V. V. 1995, *ApJ*, 452, L45

Fitzpatrick, E. L. & Walborn, N. R. 1990, *AJ*, 99, 1483

Fransson, C. & Chevalier, R. A. 1987, *ApJ*, 322, L15

Garmire, G. P., Bautz, M. W., Ford, P. G., Nousek, J. A., & Ricker, Jr., G. R. 2003, in “X-Ray and Gamma-Ray Telescopes and Instruments for Astronomy”, Proc. of SPIE, eds. J. E. Trümper and H. D. Tananbaum, 4851, 28

Garnavich, P., Kirshner, R., & Challis, P. 1997, *IAU Circ.*, 6710

Hasinger, G., Aschenbach, B., & Trümper, J. 1996, *A&A*, 312, L9

Jakobsen, P., Albrecht, R., Barbieri, C., Blades, J. C., Boksenberg, A., Crane, P., Deharveng, J. M., Disney, M. J., Kamperman, T. M., King, I. R., Macchetto, F., Mackay, C. D., Paresce, F., Weigelt, G., Baxter, D., Greenfield, P., Jedrzejewski, R., Nota, A., Sparks, W. B., Kirshner, R. P., & Panagia, N. 1991, *ApJ*, 369, L63

Kirshner, R. P., Sonneborn, G., Crenshaw, D. M., & Nassiopoulos, G. E. 1987, *ApJ*, 320, 602

Koshiba, M., Thomas, M., Ryder, S., Steeman, F., Schwarz, H.-E., Monderen, P., Seargent, D., McNaught, R. H., & Beresford, T. 1987, *IAU Circ.*, 4338

Lucy, L. B. 1974, *AJ*, 79, 745

Lundqvist, P. & Fransson, C. 1991, *ApJ*, 380, 575

Lundqvist, P. & Fransson, C. 1996, *ApJ*, 464, 924

Luo, D. & McCray, R. 1991, *ApJ*, 379, 659

Manchester, R. N., Gaensler, B. M., Wheaton, V. C., Staveley-Msmith, L., Tzioumis, A. K., Bizunok, N. S., Kesteven, M. J., & Reynolds, J. E. 2002, *PASA*, 19, 207

Masai, K. & Nomoto, K. 1994, *ApJ*, 424, 924

McCray, R. 2004, in “Supernovae”, Proc. IAU Colloquium No. 192, eds. J. M. Marcaide and K. W. Weiler, (New York: Springer Verlag), in press

McKee, C. F. & Cowie, L. L. 1977, *ApJ*, 215, 213

Michael, E., McCray, R., Pun, C. S. J., Garnavich, P., Challis, P., Kirshner, R. P., Raymond, J., Borkowski, K., Chevalier, R., Filippenko, A. V., Fransson, C., Lundqvist, P., Panagia, N., Phillips, M. M., Sonneborn, G., Suntzeff, N. B., Wang, L., & Wheeler, J. C. 2000, *ApJ*, 542, L53

Michael, E., Zhekov, S. A., McCray, R., Hwang, U., Burrows, D. N., Park, S., Garmire, G. P., Holt, S. S., & Hasinger, G., 2002, *ApJ*, 574, 166

Mori, K., Tsunemi, H., Miyata, E., Baluta, C. J., Burrows, D. N., Garmire, G. P., & Chartas, G. 2001, in “New Century of X-Ray Astronomy”, *ASP Conf. Ser.*, eds. H. Inoue and H. Kunieda (San Francisco: ASP), 251, 576

Park, S., Burrows, D. N., Garmire, G. P., Nousek, J. A., McCray, R., Michael, E., & Zhekov, S. A. 2002, *ApJ*, 567, 314

Park, S., Zhekov, S. A., Burrows, D. N., McCray, R., Garmire, G. P., & Hasinger, G. 2004, *AdSpR*, in press

Pun, C. S. J., Sonneborn, G., Bowers, C., Gull, T., Heap, S., Kimble, R., Maran, S., & Woodgate, B. 1997, *IAU Circ.*, 6665

Richardson, W. H. 1972, *J. Opt. Soc. Am.*, 62, 55

Russell, S. C. & Dopita, M. A. 1992, *ApJ*, 384, 508

Sonneborn, G., Altner, B., & Kirshner, R. P. 1987, *ApJ*, 323, L35

Townsley, L. K., Broos, P. S., Garmire, G. P., & Nousek, J. A. 2000, *ApJ*, 534, L139

Townsley, L. K., Broos, P. S., Chartas, G., Moskalenko, E., Nousek, J. A., & Pavlov, G. G. 2002a, *Nucl. Instrum. Methods Phys. Res. A*, 486, 716

Townsley, L. K., Broos, P. S., Nousek, J. A., & Garmire, G. P. 2002b, *Nucl. Instrum. Methods Phys. Res. A*, 486, 751

Tsunemi, H., Mori, K., Miyata, E., Baluta, C., Burrows, D. N., Garmire, G. P., & Chartas, G. 2001, *ApJ*, 554, 496

Weisskopf, M. C., O’dell, S. L., & van Speybroeck, L. P. 1996, in “Multilayer and Grazing Incidence X-Ray/EUV Optics III”, *Proc. of SPIE*, eds. R. B. Hoover and A. B. Walker, 2805, 2

Table 1. *Chandra*/ACIS Observations of SNR 1987A

Observation ID	Date (Age ^a)	Instrument	Exposure (ks)	Source Counts
124+1387 ^b	1999-10-06 (4609)	ACIS-S + HETG	116	690
122	2000-01-17 (4711)	ACIS-S3	9	607
1967	2000-12-07 (5038)	ACIS-S3	99	9031
1044	2001-04-25 (5176)	ACIS-S3	18	1800
2831	2001-12-12 (5407)	ACIS-S3	49	6226
2832	2002-05-15 (5561)	ACIS-S3	44	6429
3829	2002-12-31 (5791)	ACIS-S3	49	9274

^aDay since the SN explosion.

^bThe first observation was split into two sequences, which were combined in the analysis.

Table 2. Best-fit Elemental Abundances.

Element	Abundance ^a	Element	Abundance ^a
He	2.57 (fixed)	Si	$0.32^{+0.07}_{-0.06}$
C	0.09 (fixed)	S	$0.76^{+0.24}_{-0.23}$
N	$0.45^{+0.10}_{-0.09}$	Ca	0.34 (fixed)
O	$0.10^{+0.02}_{-0.01}$	Ar	0.54 (fixed)
Ne	$0.22^{+0.03}_{-0.03}$	Fe	$0.13^{+0.02}_{-0.02}$
Mg	$0.16^{+0.04}_{-0.04}$	Ni	0.62 (fixed)

^aAbundances with respect to Solar.

Table 3. Best-fit Shock Parameters^a

Date	Electron Temperature (keV)	Ionization Timescale (10^{10} cm $^{-3}$ s)	Emission Measure (10^{57} cm $^{-3}$)
2000-12-7	$2.59^{+0.25}_{-0.21}$	$3.27^{+0.66}_{-0.50}$	$6.81^{+0.42}_{-0.48}$
2001-12-12	$2.43^{+0.43}_{-0.31}$	$3.04^{+0.70}_{-0.52}$	$9.99^{+0.69}_{-0.78}$
2002-5-15	$2.22^{+0.38}_{-0.28}$	$3.46^{+0.82}_{-0.60}$	$12.00^{+0.93}_{-0.93}$
2002-12-31	$2.13^{+0.21}_{-0.15}$	$3.38^{+0.63}_{-0.50}$	$16.05^{+0.99}_{-1.17}$

^a $\chi^2/\nu = 359.0/352$

Table 4. Results from the Two-Temperature Model Fit as of 2002-12^a

Parameters	Soft Component (CIE)	Hard Component (NEI)
N_H (10^{21} cm $^{-2}$)	$2.3^{+0.6}_{-0.5}$	$2.3^{+0.6}_{-0.5}$
kT_e (keV)	$0.22^{+0.05}_{-0.02}$	$2.44^{+0.27}_{-0.23}$
$n_e t$ (10^{10} cm $^{-3}$ s)	-	$4.38^{+1.42}_{-0.88}$
EM^b (10^{57} cm $^{-3}$)	$59.78^{+10.71}_{-10.23}$	$14.25^{+0.60}_{-0.57}$
f_X^c (10^{-13} ergs cm $^{-2}$ s $^{-1}$)	$1.57^{+0.28}_{-0.27}$	$7.22^{+0.30}_{-0.29}$
L_X^c (10^{35} ergs s $^{-1}$)	1.61	3.72

^a $\chi^2/\nu = 94.29/99$.

^bThe uncertainties were estimated after fixing N_H and kT at the best-fit values.

^cThe X-ray fluxes and luminosities were estimated in the 0.5–10.0 keV band.

Table 5. X-ray Fluxes for the Eastern and Western sides of SNR 1987A.

	2000-12		2002-12	
	East	West	East	West
Soft Component ^a	$0.43^{+0.07}_{-0.08}$	$0.17^{+0.04}_{-0.04}$	$0.58^{+0.25}_{-0.25}$	$0.92^{+0.16}_{-0.19}$
Hard Component ^a	$1.92^{+0.16}_{-0.13}$	$1.46^{+0.09}_{-0.11}$	$4.07^{+0.43}_{-0.43}$	$3.10^{+0.33}_{-0.26}$

^aThe 0.5–10 keV band fluxes in units of 10^{-13} ergs cm^{-2} s^{-1} . The uncertainties were estimated after fixing N_H and abundances at the best-fit values presented in Table 2 and Table 4.

Table 6. The 0.5–2.0 keV band flux of SNR 1987A.

Age ^a (days)	Observed Flux (<i>ROSAT</i>) (10^{-13} ergs cm^{-2} s^{-1})	Age ^a (days)	Observed Flux (<i>Chandra</i>) (10^{-13} ergs cm^{-2} s^{-1})
1215	<0.23	4609	1.62 ± 0.06
1448	0.07 ± 0.09	4711	1.74 ± 0.07
1645	0.15 ± 0.04	5038	2.59 ± 0.03
1872	0.19 ± 0.04	5176	2.93 ± 0.07
2258	0.27 ± 0.05	5407	3.82 ± 0.05
2408	0.32 ± 0.07	5561	4.45 ± 0.06
2715	0.33 ± 0.11	5791	5.95 ± 0.06
3013	0.41 ± 0.06		

^aDays since the SN explosion.

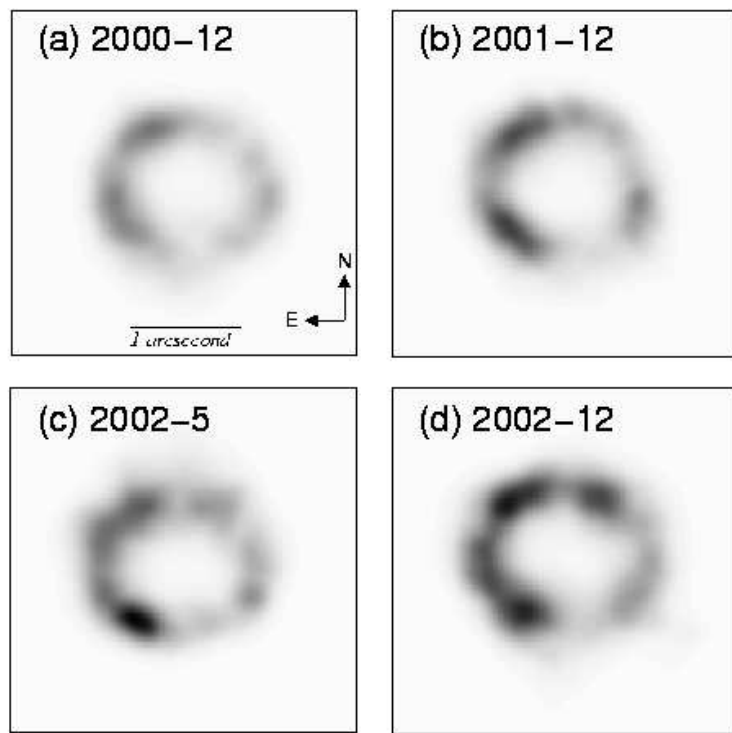


Fig. 1.— The gray-scale 0.3–8.0 keV broadband images of SNR 1987A. each image is exposure-corrected and the darker gray-scale is higher flux. The image deconvolution has been applied and then the images have been smoothed by convolving with a Gaussian ($\sim 0''.1$ FWHM).

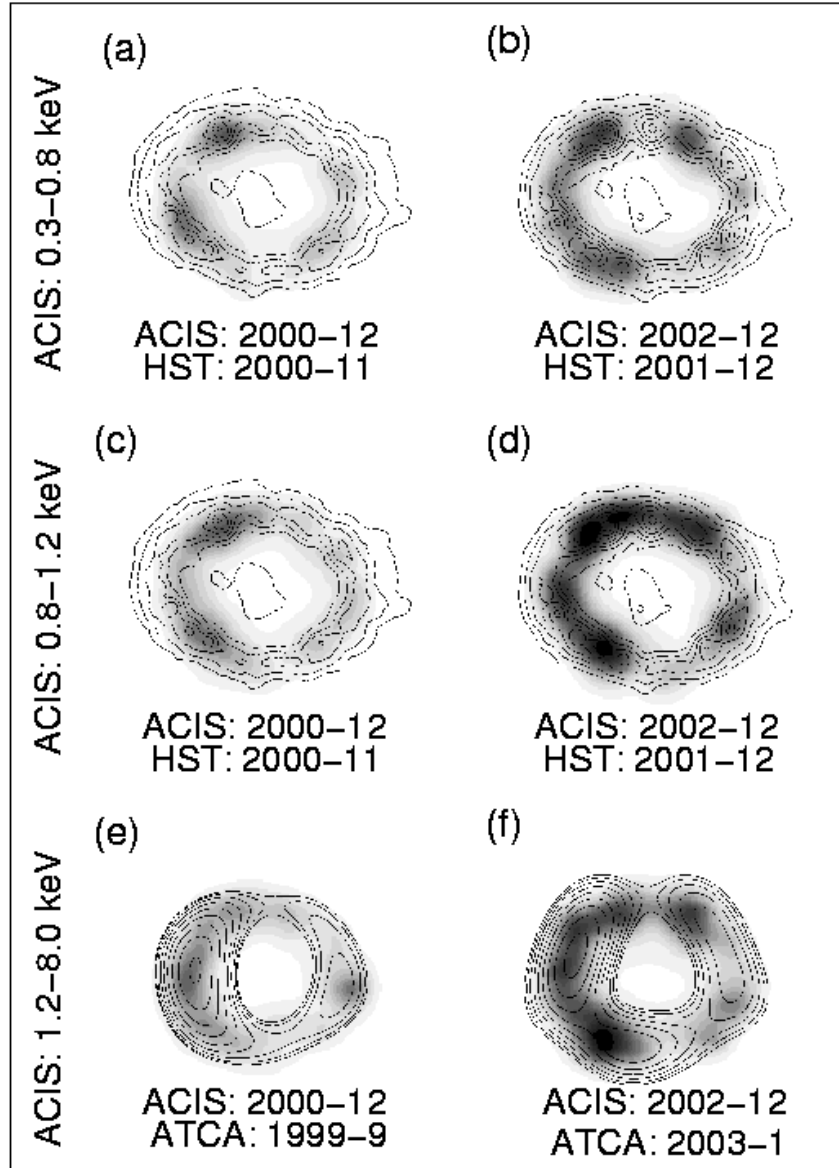


Fig. 2.— The broad sub-band ACIS images of SNR 1987A. Each image has been processed in the same way as those in Figure 1. The *HST* contours are overlaid with the O-band (0.3–0.8 keV) and the Ne-band (0.8–1.2 keV) ACIS images. The 9 GHz radio contours taken by Australian Telescope Compact Array (ATCA) are overlaid with the H-band (1.2–8.0 keV) ACIS images.

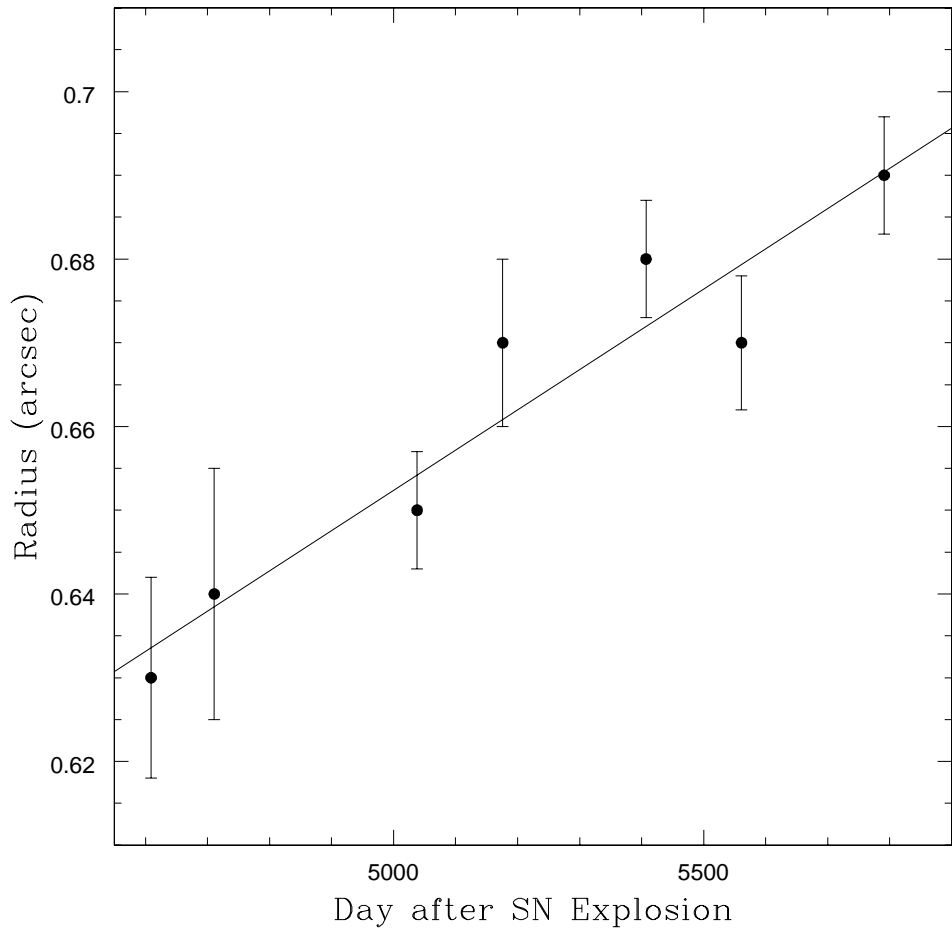


Fig. 3.— The long-term variation of the mean radius of the X-ray count distribution as obtained with a Gaussian fit. The solid line is the best-fit linear increase rate representing an expansion velocity of ~ 4167 km s $^{-1}$.

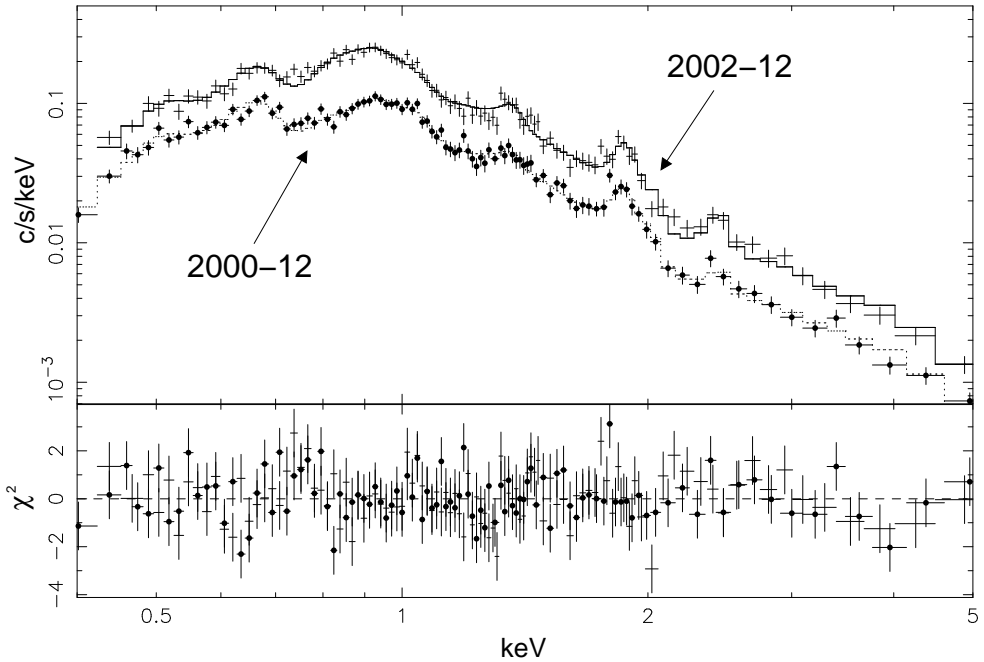


Fig. 4.— The X-ray spectrum of SNR 1987A. The best-fit single NEI model is overlaid for each spectrum taken on 2000-12 and 2002-12.

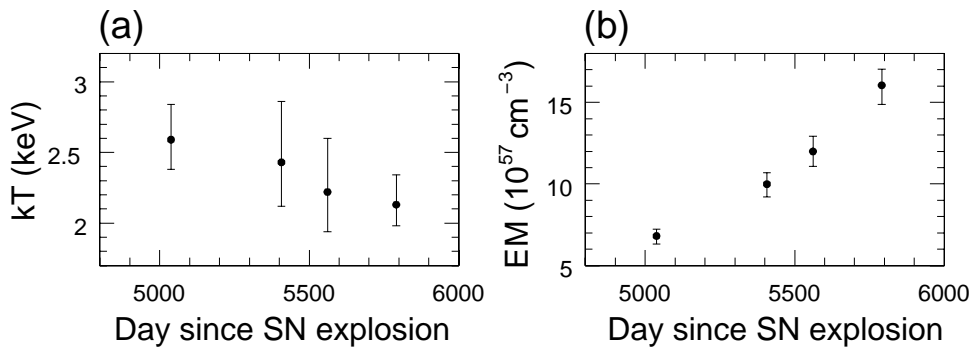


Fig. 5.— The electron temperature and the emission measure variations of SNR 1987A between 2000-12 and 2002-12.

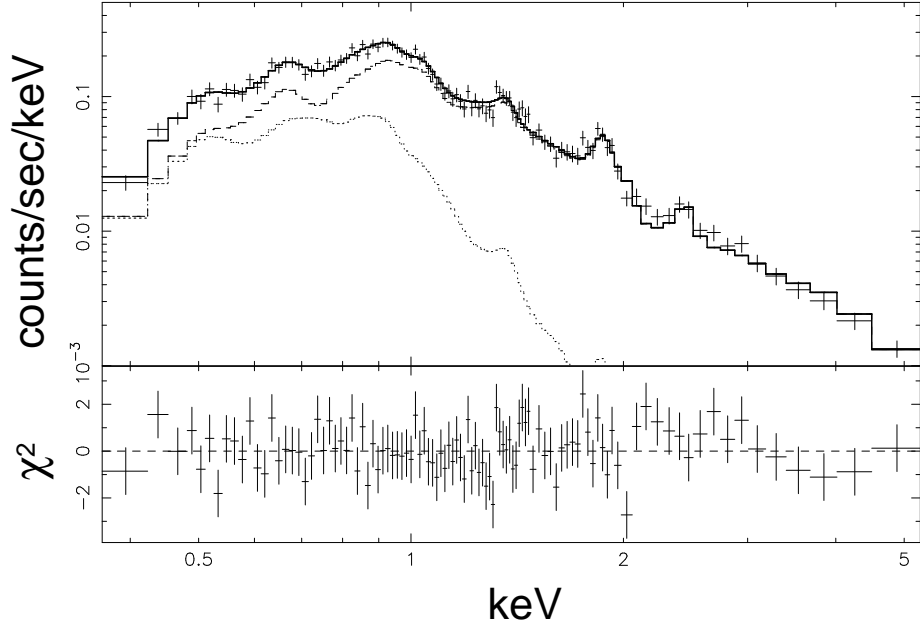


Fig. 6.— The X-ray spectrum of SNR 1987A as of 2002-12. The best-fit two-temperature model is overlaid.

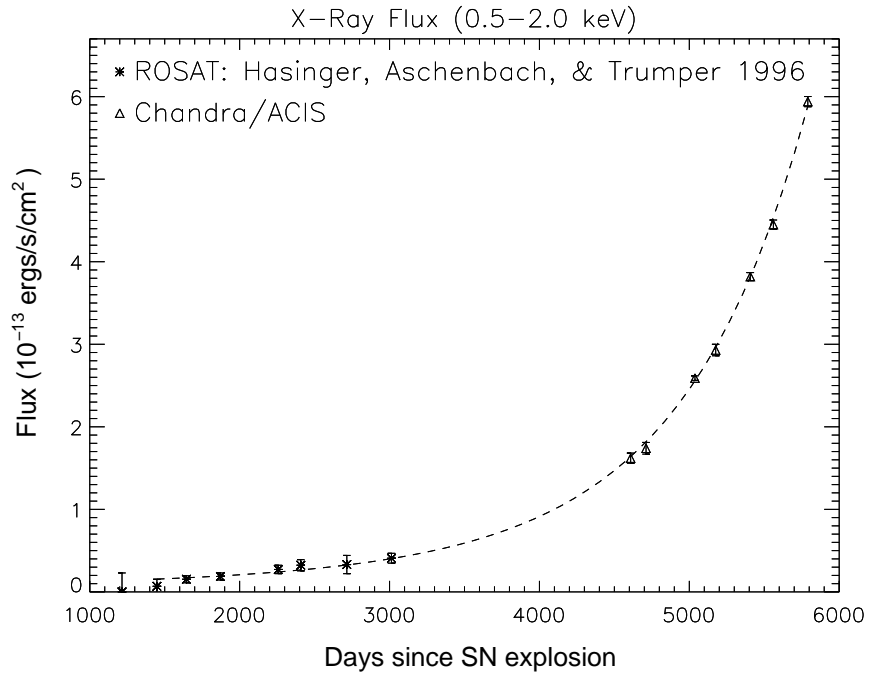


Fig. 7.— The X-ray light curve of SNR 1987A. The best-fit model with an exponential density distribution is overlaid with a dashed curve.